This article has been accepted for publication in a future issue of this journal, but has not been fully edited. Content may change prior to final publication. Citation information: DOI 10.1109/TAP.2017.2670362, IEEE Transactions on Antennas and Propagation

Wideband Multimode Monostatic Spiral Antenna STAR Subsystem

Ehab A. Etellisi, *Student Member, IEEE*, Mohamed A. Elmansouri, *Member, IEEE*, and Dejan S. Filipović, *Senior Member, IEEE*

***Abstract*— A wideband, multimode, and monostatic simultaneous transmit and receive (STAR) antenna subsystem is proposed. The configuration is composed of a single four-arm spiral and two analog circuit layers designed to maximize isolation between the transmitting (TX) and receiving (RX) channels. The first layer consists of two Butler matrix beamformer networks (BFNs); one for each TX, and RX. The second layer integrates four, ideally phase-matched, circulators between the spiral arms and the BFNs. Theoretically, this configuration achieves infinite isolation irrespective of circulator's quality. However, the BFN imbalances and the dissimilarities between the four circulators degrade the overall isolation. The operational principles are discussed under the ideal conditions and in the presence of circuit imperfections. For a four-arm spiral, the utilized BFN provides orthogonal modes 1, -1, 2, and 3 allowing STAR capability with multimode and diverse radiation patterns. The subsystem isolation and far-field performances are characterized experimentally and computationally for different modes of operation. A simple approach to achieve a dual-polarized STAR operation over narrower bandwidth with the proposed subsystem is also discussed. The multimode subsystem is demonstrated over 4:1 bandwidth with high isolation, VSWR<2, consistent patterns, axial ratio<3dB over a wide field of view for the broadside modes (1, -1) and <4.2dB for other conical modes (2, 3).**

***Index Terms*—Butler-matrix, circulators, full-duplex, isolation, self-interference cancellation, spiral antenna, STAR**

I. Introduction

Wireless networks typically operate in half-duplex regime where they transmit and receive over the same real-estate at different times or frequencies using either time or frequency division duplex (TDD or FDD) [1]. To improve the throughput and spectral efficiency of the existing wireless networks and maximize RF spectrum use, full-duplex or simultaneous transmit and receive (STAR) systems have been recently considered [2]-[9]. Realizing STAR operation with a single aperture is challenging due to the high self-interference, which disables the receiver's ability to discern the actual signal. To eliminate the self-interference problems, the TX/RX system isolation is required to be high, typically >100dB for low-TX powers. This high isolation level is typically achieved by utilizing multiple stages of self-interference cancellations in antenna, analog, and digital domains [10]. This paper proposes a novel wide bandwidth single-aperture STAR antenna subsystem with high isolation and attractive radiation characteristics for different applications.

Typical approaches for achieving high isolation at the antenna layer rely on physically separating the TX and RX apertures by several wavelengths [2], dissimilar beam orientations, polarization differentiation, self-cancelation with manipulation of the phases of coupling paths, or null placement in the direction of RX antenna [3]-[9]. These techniques can achieve tolerable levels of isolation at the expense of large size, narrow bandwidth, complex BFN, different TX and RX radiation characteristics, and high cost making them unrealistic for many wireless systems. For all these reasons, single aperture STAR antenna subsystems are vastly preferred.

Single aperture subsystems usually utilize passive ferrite circulators to isolate the TX and RX paths. These circulators are inherently narrowband; however, the bandwidth thereof can be improved to two octaves [11] at expense of lower isolation (<15dB) and higher insertion loss (>1.5dB). State of the art commercial-of-the-shelf (COTS) circulators can achieve high isolation level of >20dB over an octave bandwidth [12]. However, the return loss of the antenna limits their use due to the leaked reflected signal. Thus, the use of these high-isolation circulators for monostatic STAR applications requires an antenna with return loss better than the circulator's isolation over the entire operating bandwidth, which is quite challenging. In addition to passive circulators [13]-[16], active electronic and photonic circulators are demonstrated [17]-[20]. These devices outperform their passive counterparts in terms of isolation and bandwidth and a decade bandwidth photonic circulator with isolation >40dB is achievable [20]. This device has an additional port, antenna-balance port, which balances out the impedance variation of the antenna and overcomes the issue of leakage due to the antenna reflection. The recognized drawbacks of the photonic as well as active circulators include complexity, limited power handling capability, linearity, size and higher cost.

Other interesting techniques to realize monostatic STAR subsystems are also proposed [21]-[22]. Therein, spiral antenna geometrical characteristics and applied excitation are

The authors are with the Department of Electrical, Computer, and Energy Engineering, University of Colorado, Boulder, CO 80309-0425 USA (e-mail: {ehab.etellisi, mohamed.elmansouri, dejan}@colorado.edu).

This work is supported by the Office of Naval Research (ONR) award # N00014-15-1-2125.

This article has been accepted for publication in a future issue of this journal, but has not been fully edited. Content may change prior to final publication. Citation information: DOI 10.1109/TAP.2017.2670362, IEEE Transactions on Antennas and Propagation

exploited to cancel the coupled TX signal at the RX port. These circulator-less techniques have shown isolation >38dB over 5:1 bandwidth. However, the STAR spiral's far-field performance (i.e. axial ratio and gain) is degraded at lower frequencies compared to the performance of a conventional spiral due to the existence of the parasitic arms. Other techniques implement a balanced feed network of two circulators and quadrature hybrids capable of simultaneously cancelling the circulator leakage and the antenna reflection are proposed in [23]-[24]. In [24], isolation >40dB is demonstrated over the designated bandwidth from 900MHz-930MHz. The system bandwidth is limited by the used components' operational bandwidth and performance quality.

This paper proposes a novel monostatic approach that fully exploits the characteristics of a four-arm spiral, its BFN and circulators to achieve high isolation. Since the introduced configuration utilizes a single multi-mode frequency-independent antenna the multi-octave operation with decent far-field performance and cost-effective implementation is enabled. Different polarization and modes of operation with broadside or conical radiation characteristics can also be supported. Moreover, high power handling capability can be achieved by implementing a robust spiral design [22] and utilizing high-power circulators and hybrids. The subsystem architecture and principle of operation are fully discussed in this paper. The impact of circuit component imperfections on the overall TX/RX isolation is also analyzed. Furthermore, the demonstration STAR spiral subsystem is prototyped and measured with actual components to showcase the practical feasibility of the proposed antenna subsystem.

This paper is organized as follows; Section II discusses the operational principle of the proposed multimode STAR antenna subsystem. Section III shows the impact of circuitry's imbalances and asymmetry on the TX-RX isolation. Section-IV describes the realized antenna subsystem and characterizes the performance thereof for mode 1 operation. Finally, the feasibility of multimode STAR operation is discussed in Section V.

II. STAR Antenna Subsystem Description and Operational Principles

The proposed monostatic STAR antenna subsystem is shown in Fig. 1. The subsystem consists of a single four-arm spiral aperture and two Butler matrix BFNs (i.e. one for TX channel and the other for RX channel). Phase-matched circulators are integrated on each arm between the antenna and BFNs. The main components of the subsystem are:

Antenna: Four-arm spiral is employed to achieve wideband operation with good and consistent impedance match, and stable radiation patterns. This antenna can also support three different frequency independent modes. Each mode has its own input impedance and far-field characteristics. Mainly, mode 1 (broadside mode) and modes 2 and 3 (conical beam modes) can be excited by applying equal amplitude and proper phase vector splits between spiral arms. Particularly, to excite mode *m* of operation the relative phase between spiral arms has to be $m\pi/2$ [25]. Notice that the turn-on frequencies of modes 2 and 3 are two and three times the turn-on frequency of mode 1; respectively. The multimode capability is crucial for the antenna subsystem performance, as it will be demonstrated. Another interesting feature of this aperture is the ability to radiate both senses of circular polarization (i.e. RHCP and LHCP) over ~3:1 bandwidth if it is appropriately designed and excited [25]. The dual-polarized spiral principle of operation is based on the support of mode 3 which will not radiate efficiently until three times mode 1 turn-on frequency due to the size of the used spiral aperture. Thus, the non-radiating currents reach the open end of spiral arms and reflect back as mode -1 which then radiates with the opposite polarization sense of mode 1. This feature will be utilized to demonstrate a dual-polarized monostatic STAR antenna subsystem. The proposed approach works with any four-arm spiral topology either a planar or a conical spiral. Right-handed wrapped Archimedean spiral is selected herein for further discussion and demonstration.

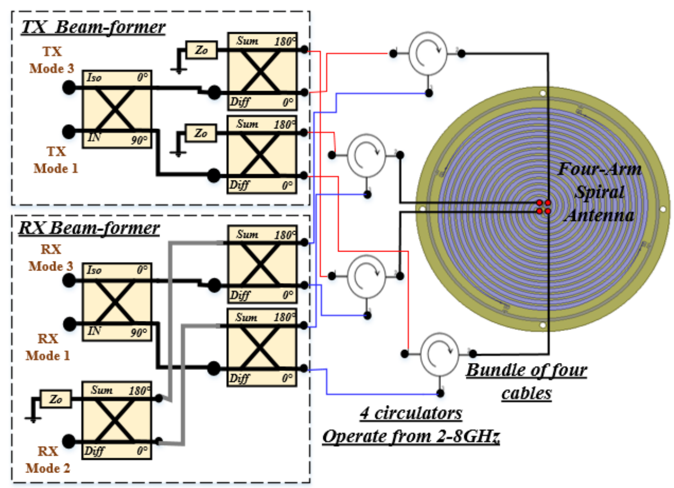

Fig. 1. Schematic of the proposed STAR antenna subsystem.

Circulators: Four ferrite circulators are connected to the four-arm spiral through a bundle of four coaxial cables. The other two circulators' ports are connected to the TX and RX BFNs as shown in Fig.1. Circulators are employed to realize a monostatic STAR operation; however, they can be replaced with power dividers, directional couplers, or other three port routing device [24]. The circulators are chosen here since they provide the lowest insertion loss for both TX and RX paths. Theoretically, as will be shown later, the proposed STAR antenna subsystem can achieve infinite isolation irrespective of the circulator's quality. However, it is important that the four circulators are phase-matched to avoid any extra imbalances that could degrade the isolation. Also, it should be noted that the circulator bandwidth limits the proposed system's operational bandwidth.

Beamforming Network (BFN): 2(inputs)×4(outputs) Butler matrix BFN consisting of two 180º hybrids and one 90º hybrid is used at the TX side as shown in Fig. 1. TX BFN supports the excitation of modes 1 and 3. The RX BFN is 4× 4 Butler matrix BFN. It consists of three 180º hybrids and one 90º hybrid as shown in Fig. 1. The RX BFN supports the excitation of modes 1, 2, 3, and 4. Mode 4 is unused in this configuration and its port is terminated with a matched load. The proposed STAR antenna subsystem can operate in broadside beam mode 1 or conical beam mode 3

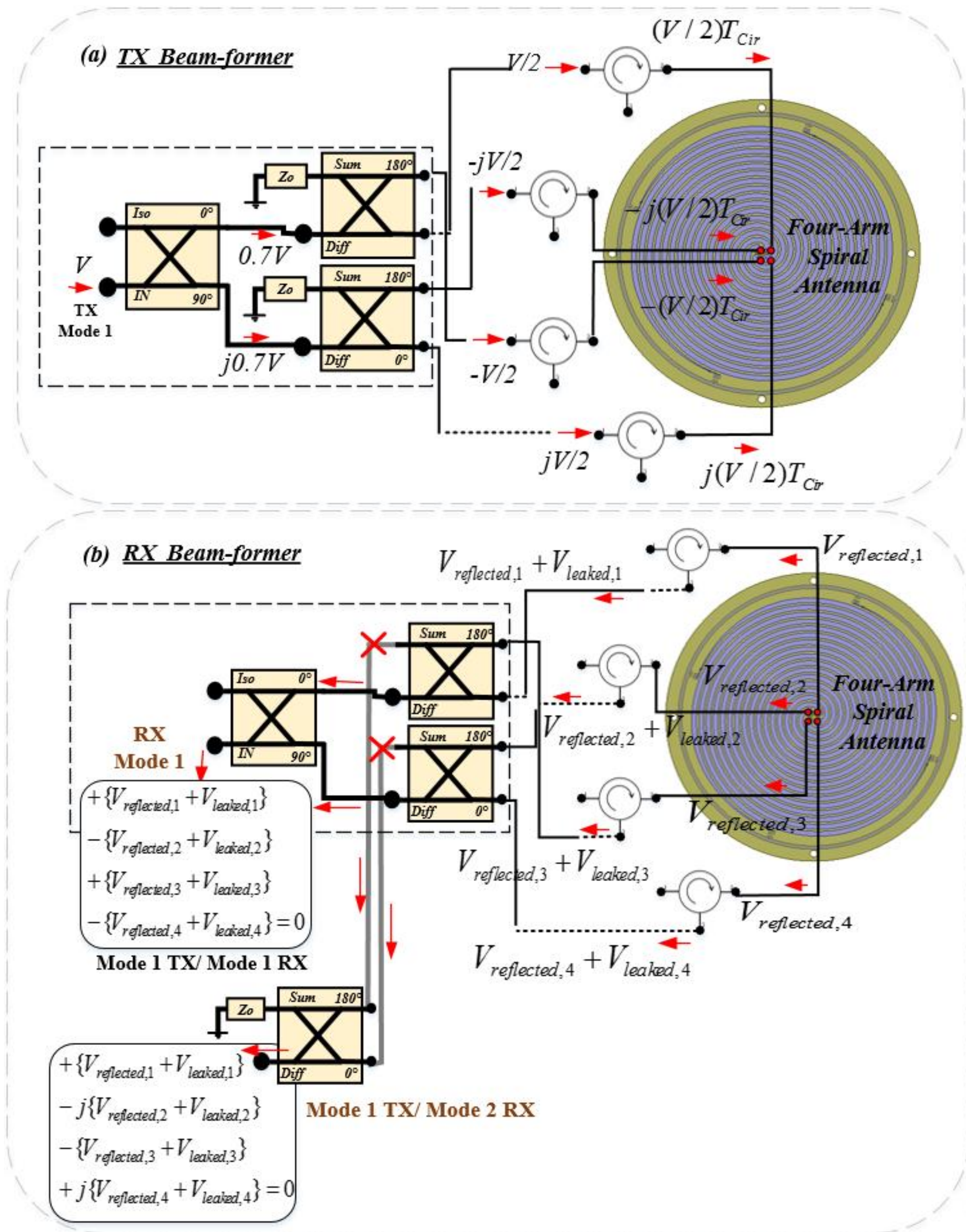

Fig. 2. Signal flow diagram of the proposed STAR subsystem for (a) TX, and (b) RX sides. TX BFN supports the excitation of modes 1 and (3,-1) and the RX BFN supports the excitation of modes 1, 2, and (3,-1). Only (Mode 1) TX and (Mode 1 and Mode 2) RX coupling signal cancellation mechanism is shown. For (mode 3 or mode -1) TX and (mode 3 or mode -1) RX, the analysis is similar but the feeding port is switched at the TX and RX 90° hybrids.

with similar RHCP TX and RX radiation patterns. Different TX and RX patterns can also be obtained by operating the TX and RX BFNs in modes 1 and 2; respectively. Moreover, LHCP broadside patterns can be radiated by exciting mode -1 (i.e. mode 3 below its turn-on frequency) at TX and RX BFNs. For all these arrangements, high isolation is preserved between the TX and RX channels. If the antenna is fully symmetric and TX/RX BFNs are ideal (i.e. imbalances-free), the proposed subsystem should completely eliminate the self-interference at RX port and re-route the coupled TX signal to the unused input ports.

To demonstrate the STAR antenna subsystem operational principles, the signal flow from the TX port to the RX port is analyzed as shown in Fig. 2. To simplify the analysis, lossless ideal hybrids and phase-matched circulators are assumed. The principle of operation for each TX/RX mode is explained as follows:

A. Mode 1 TX / Mode 1 RX: For mode 1 operation at TX and RX sides, the antenna subsystem isolation can be computed by accounting for all coupling paths as:

1) Starting from TX BFN, mode 1 port is excited with a voltage signal of magnitude V. The output voltages can be simply written as:

$$V_{TX,n} = (\,V/\,2)\;e^{-j\phi_{TX,n}} \tag{1.a}$$

and

$$\phi_{TX,n} = \{0°, \pi/2, \pi, 3\pi/2\}\;;\; n = 1,2,3,\text{and } 4 \tag{1.b}$$

The four output signals have eqaul magnitude of (V/2) and phase vector of ϕ_{TX}.

2) The output signals are routed by the circulators to the antenna ports which enabling mode 1 radiation. Portion of the signal ($V_{leaked,n}$) is leaked to the RX paths due to the insufficient isolation of the circulator. The input signal to each spiral arm is defined as,

$$V_{input,n} = V_{TX,n}\,\mathrm{T}_{Cir.,n} \tag{2}$$

and the leaked signal,

$$V_{leaked,n} = V_{TX,n}\,\mathrm{L}_{Cir.,n} \tag{3}$$

where $\mathrm{T}_{Cir.,n}$ and $\mathrm{L}_{Cir.,n}$ are the circulator transmission coefficient and leakage factor, respectively. Then, the reflected TX signal from the antenna arms ($V_{reflected,n}$) couples through the circulators to the RX paths as shown in Fig. 2b,

$$V_{reflected,n} = V_{input,n}\;\Gamma_{arm,n}\,\mathrm{T}_{Cir.,n} \tag{4}$$

where $\Gamma_{arm,n}$ is the active reflection coefficient of each antenna's arm.

3) The TX coupled signals from the spiral reflection ($V_{reflected,n}$) and circulators leakage ($V_{leaked,n}$) are then routed through the RX BFN. The coupled TX signals at RX port can be written as,

$$C_{1\_(TX\ to\ RX)} = \left(\frac{1}{2}\right)\left(V_{leaked,1} + V_{reflected,1}\right)e^{-j\{0\}} \tag{5.a}$$

$$C_{2\_(TX\ to\ RX)} = \left(\frac{1}{2}\right)\left(V_{leaked,2} + V_{reflected,2}\right)e^{-j\{\pi/2\}} \tag{5.b}$$

$$C_{3\_(TX\ to\ RX)} = \left(\frac{1}{2}\right)\left(V_{leaked,3} + V_{reflected,3}\right)e^{-j\{\pi\}} \tag{5.c}$$

$$C_{4\_(TX\ to\ RX)} = \left(\frac{1}{2}\right)\left(V_{leaked,4} + V_{reflected,4}\right)e^{j\{\pi/2\}} \tag{5.d}$$

By plugging (3) and (4) in (5), the previous equation can be simplifed further and re-written as,

$$C_{1\_(TX\ to\ RX)} = \left(\frac{V}{4}\right)\left(L_{Cir.,1} + \mathrm{T}_{Cir.,1}\;\Gamma_{arm,1}\,\mathrm{T}_{Cir.,1}\right) \tag{6.a}$$

$$C_{2\_(TX\ to\ RX)} = \left(\frac{-V}{4}\right)\left(L_{Cir.,2} + \mathrm{T}_{Cir.,2}\;\Gamma_{arm,2}\,\mathrm{T}_{Cir.,2}\right) \tag{6.b}$$

$$C_{3\_(TX\ to\ RX)} = \left(\frac{V}{4}\right)\left(L_{Cir.,3} + \mathrm{T}_{Cir.,3}\;\Gamma_{arm,3}\,\mathrm{T}_{Cir.,3}\right) \tag{6.c}$$

$$C_{4\_(TX\ to\ RX)} = \left(\frac{-V}{4}\right)\left(L_{Cir.,4} + \mathrm{T}_{Cir.,4}\;\Gamma_{arm,4}\,\mathrm{T}_{Cir.,4}\right) \tag{6.d}$$

4) If the symmetry is maintained along all circulators; the TX and RX BFNs, and active reflection coefficients of the four spiral antenna's arms, are assumed to be similar as,

$$L_{Cir.,1} = L_{Cir.,2} = L_{Cir.,3} = L_{Cir.,4} \tag{7.a}$$

$$\mathrm{T}_{Cir.,1} = \mathrm{T}_{Cir.,2} = \mathrm{T}_{Cir.,3} = \mathrm{T}_{Cir.,4} \tag{7.b}$$

$$\Gamma_{arm,1} = \Gamma_{arm,2} = \Gamma_{arm,3} = \Gamma_{arm,4} \tag{7.c}$$

5) These routed coupled signals in (6) should cancel one another since each two coupling paths are out of phase compared to the other two. Then, the total routed coupled signals from the TX ports to the RX port can be expressed as (8.a).

$$C_{(TX\ to\ RX)} = C_{1\_(TX\ to\ RX)} + C_{2\_(TX\ to\ RX)} + C_{3\_(TX\ to\ RX)} + C_{4\_(TX\ to\ RX)} = 0 \tag{8.a}$$

Or, in more general form as

$$C_{(TX\ to\ RX)} = \left(\frac{1}{2}\right)\sum_{n=1}^{4}\left(V_{leaked,n} + V_{reflected,n}\right)\,e^{-j\phi_{RX(n)}} = 0 \tag{8.b}$$

Where

$$\phi_{RX(n)} = \{0°, \pi/2, \pi, 3\pi/2\}\ ;\ n = 1,2,3,4 \tag{8.c}$$

Hence, the BFNs effectively cancel portion of the coupled TX signals that travel to the RX port; while redirecting the rest of the non-radiated coupled signals from the transmitter to the unused mode 3 port of the RX 90° hybrid which is appropriately terminated.

B. Mode 3 TX / Mode 3 RX & Mode -1 TX / Mode -1 RX : for this arrangement, the other port of the *90°* hybrids in both TX and RX BFNs is used to excite mode 3 (higher band) and mode -1 (lower band), as illustrated in Fig.1. It can be proven that the TX coupled signals are also cancelled for TX/RX mode 3 and mode -1 operation and the residual signals are redirected to the RX BFN mode 1 port. Even though the signal flow is not included in Fig.2, the similar analysis to Mode 1 can be easily repeated. Only, the TX and RX phase progressions of (1.b) and (8.c) need to be replaced by:

$$\phi_{TX(n)} = \{0°, 3\pi/2, \pi, \pi/2\}\,;\ n = 1,2,3,4 \tag{9.a}$$

$$\phi_{RX(n)} = \{0°, 3\pi/2, \pi, \pi/2\}\,;\ n = 1,2,3,4 \tag{9.b}$$

C. Mode 1 TX / Mode 2 RX: Once mode 1 is excited as TX, mode 1 RX and mode 2 RX can be received simultaneously. For mode 1 TX / mode 2 RX configuration, the coupled mode 1 TX signals are cancelled at the sum ports of first two 180º RX hybrids before entering the last RX 180° hybrid. Hence, for the ideal case no coupled signal should be directed through the last mode 2 180º hybrid as shown in Fig. 2b. To compute the coupling, (1)-(8) can be re-applied and only the RX phase progression in (8.c) is needed to be replaced to produce mode 2 as:

$$\phi_{RX(n)} = \{0°, \pi, 0, \pi\}\,;\ n = 1,2,3,4 \tag{10}$$

The above investigation for the various modes shows that the coupled TX signals are cancelled at the receiving BFN ports leading to theoretically infinite isolation between TX and RX channels. To validate the proposed assumption computationally, the method of moments (MoM) solver FEKO, [26], is used to model a dual-layer 70mm diameter four-arm Archimedean spiral. The simulated s-parameters are then imported to AWR circuit simulator where the ideal hybrids and 10dB isolation circulators are implemented and the antenna subsystem TX/RX isolation is computed. The simulated isolation is plotted in Fig. 3 and as expected, high subsystem isolation of >75dB is obtained for the three configurations over 4:1 bandwidth.

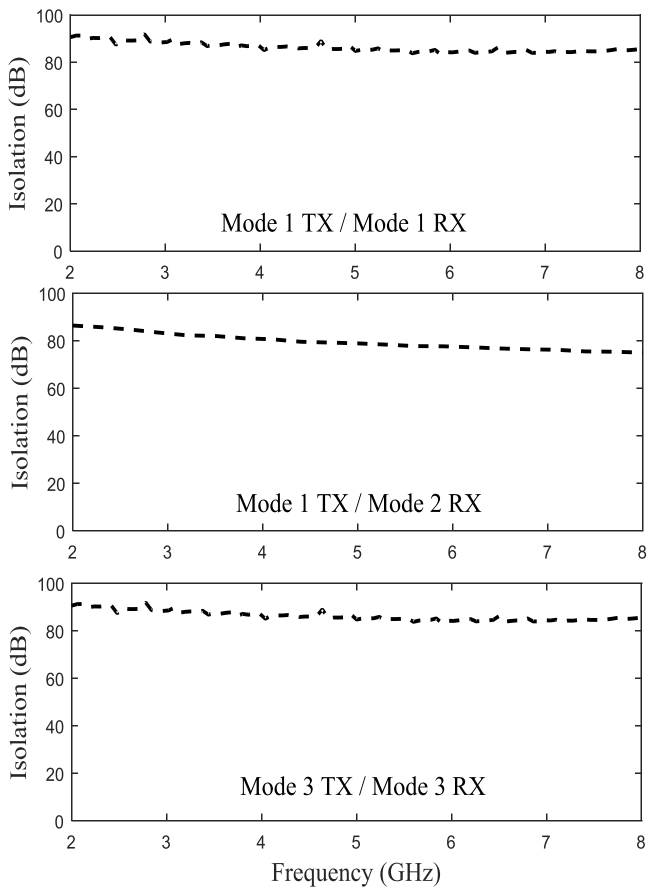

Fig. 3. Mode 1 TX / Mode 1 RX, Mode (3,-1) TX / Mode (3,-1) RX, and Mode 1 TX / Mode 2 RX simulated isolation of an ideal spiral STAR system.

III. Non-Ideality Effects

In previous section, the circuit components were assumed to be ideal. However, in practice, these components have responses that vary differently over the frequency band of operation. This indeed introduces some asymmetry to each of the TX coupled signal paths causing deterioration in the isolation performance. In other words, the general expression stated in (8.b) is no longer accurate and should be substituted by (11) to account for these imperfections.

$$C_{(TX\ to\ RX)} = \left(\frac{1}{2}\right)\sum_{n=1}^{4}\left\{V_{leaked,n} + V_{reflected,n} + V_{inc}\right\}. \\ e^{-j\left\{\phi_{RX(n)}+\phi_{RX_{inc}}\right\}} \neq 0 \quad (11)$$

where $\phi_{RX_{inc}}$ and V_{inc}, are the errors introduced by the circuit components imperfections. To investigate these effects, numerical studies are conducted by varying the isolation levels of (a) the four circulators and (b) the amplitude and phase of the hybrids. For space restrictions, only mode 1 TX / mode 1 RX configuration is considered; however, similar conclusions apply to other antenna subsystem configurations.

A. Circulators: the differences among the circulators' characteristics lead to changing the complex weights of each of the TX coupled signal paths. As a consequence, the overall isolation decreases significantly since no full-cancellation is achieved at the RX port/s. Assessment of the isolation behavior can be examined by changing each of the four matched circulators' isolation. The chosen isolation for the four circulators are 10dB, 20dB, and 30dB. Notice, the employed ideal circulators in this study are assumed to be frequency-independent just to demonstrate the overall impact. The results are shown in Fig.4a, and as seen when all circulators have identical behavior, the overall TX/RX isolation remains the same even though the isolation levels of each circulator changes from 10dB to 30dB. This result confirms our observation in (8.b). Nevertheless, once the circulators are different, the total TX/RX isolation drops from the range of 80dB-90dB into 30dB-40dB, as seen in Fig. 4b. The more the performance of the four circulators deviates from one another, the more the antenna subsystem isolation changes according to the levels of the four circulators' isolation, as shown in Fig. 4b. For instance, comparing the two cases of (C1=10dB, C2=11dB, C3=12dB, C4=13dB) with (C1=20dB, C2=21dB, C3=22dB, C4=23dB), around ~5-7dB improvement is observed.

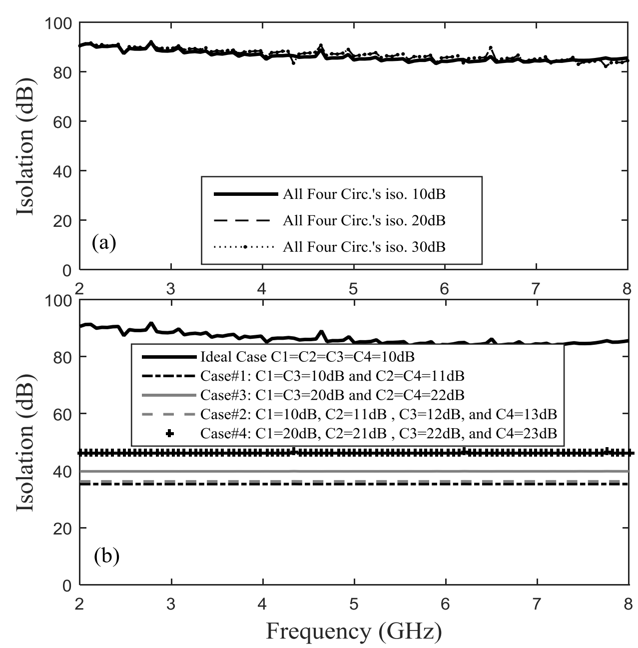

Fig. 4. The effect of the four circulators on Mode 1 TX / Mode 1 RX isolation. "C" denotes isolation of each circulator.

B. Hybrids: The impacts of amplitude and phase imbalances of the two Butler-matrices are considered next. The chosen frequency-independent amplitude and phase imbalances of the

This article has been accepted for publication in a future issue of this journal, but has not been fully edited. Content may change prior to final publication. Citation information: DOI 10.1109/TAP.2017.2670362, IEEE Transactions on Antennas and Propagation

hybrids are varied within 0dB-0.6dB and 0°-8°, respectively. The amplitude and phase errors can be introduced in circuit simulator or using (11). The TX/RX isolation study shown in Fig. 5 depicts the spread of isolation values for considered hybrids' amplitude and phase imbalances. Notice that even in the worst case isolation of 20dB, the antenna subsystem still achieves >10dB extra isolation compared to the 10dB circulators' isolation over 4:1 bandwidth. Overall, these results emphasize the importance of the circuit components on controlling the subsystem level of isolation.

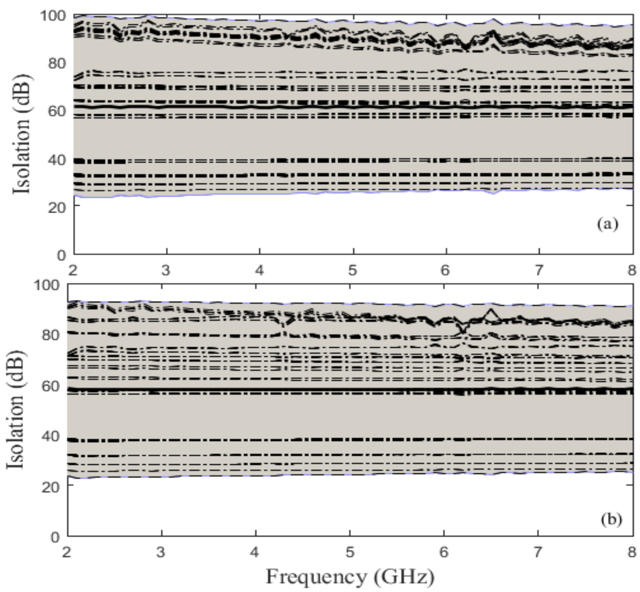

Fig. 5. Study demonstrates the effects of the hybrids' imbalances on Mode 1 TX/ Mode 1 RX isolation; (a) Amplitude, and (b) phase imbalances. The ideal circulators' isolation is fixed at 10dB.

IV. Implementation and Mode 1 Performance

To experimentally demonstrate the proposed STAR subsystem, a dual-layer right-handed four-arm Archimedean spiral with four turns is fabricated (see inset of Fig. 6). The antenna has outer and inner radii of 70mm and 2.5mm, respectively, and it was fabricated on a 0.76mm-thick Rogers 5870 Teflon based substrate ($\varepsilon_r = 2.33, tan\,\delta = 0.0012$). A 50Ω coaxial bundle composed of four semi-rigid cables is used to feed the antenna. To reduce the input impedance and achieve good impedance match with the utilized bundle, the metal to slot ratio (MSR) of the spiral is increased to 3:1. To further improve the match, the dual-layer configuration as in [27] is used; where the bottom and the top layers are connected with vias located at the center and the arms ends. The antenna aperture is backed by ECCOSORB AN-75 absorber. The mode 1 of this spiral turns-on at ~1.5GHz. The BFN is composed of five 180°, two 90° hybrids, and four circulators all operating over 2-8GHz and integrated as depicted in Fig. 1. All isolation measurements were conducted in the University of Colorado anechoic chamber. Measured and simulated active VSWRs of the fabricated spiral antenna are shown in Fig. 6. Overall active VSWR<1.7 is obtained from 2GHz-8GHz and further improvement is obtained in VSWR performance once the antenna is connected to the TX or RX circulators and BFNs. This is due to the re-routing of reflections to the terminated ports of TX and RX 90º hybrids.

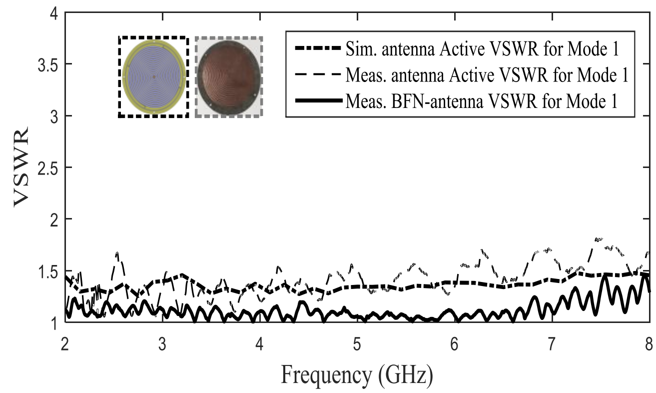

Fig. 6. Measured and simulated active VSWRs for one port of the four-arm spiral antenna. Also shown is the measured VSWR for the TX/RX circulator-BFN's ports once connected to the fabricated antenna. Shown in the inset are the computational model and the photo of the fabricated spiral aperture.

The complete layout of the mode 1 STAR antenna subsystem including the Butler matrix TX-RX BFNs, circulators, and the fabricated four-arm spiral is shown in Fig.7. Two sets of isolation measurements are conducted; one for a single circulator, and other for the entirely integrated STAR antenna subsystem (BFNs, circulators, and fabricated four-arm spiral antenna). The measured isolation for one of the four COTS circulators is around 10dB; while for (mode 1 TX / mode 1 RX) the isolation is >27dB (maximum of 38dB) with nominal of 32dB over the band.

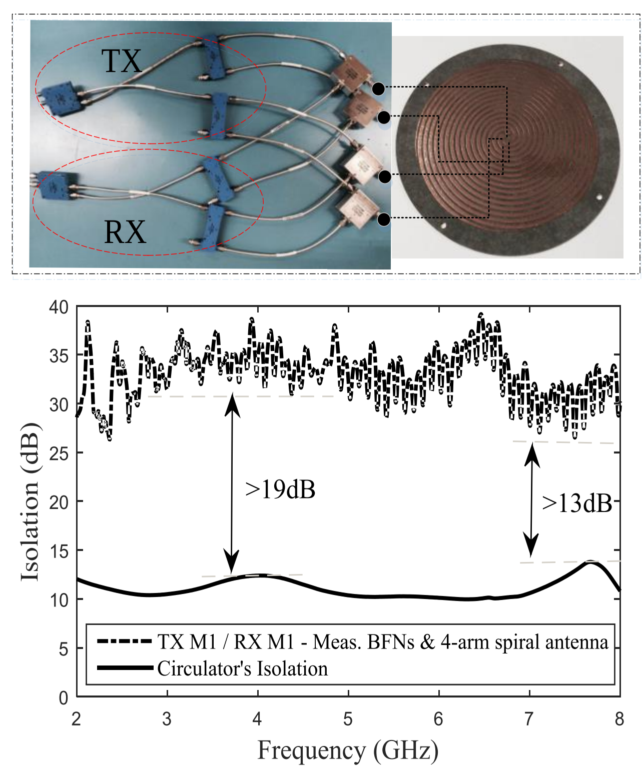

Fig. 7. Mode 1 TX / mode 1 RX measured isolation between the TX/RX BFN's ports compared to one of the four used circulators. The inset shows the STAR subsystem of mode 1 TX / mode 1 RX configuration.

As discussed in the previous section, both the imbalances of the hybrids and asymmetry of the four circulators contribute negatively on the performance of the total TX/RX isolation. Even though there is a drop in isolation with respect to the

This article has been accepted for publication in a future issue of this journal, but has not been fully edited. Content may change prior to final publication. Citation information: DOI 10.1109/TAP.2017.2670362, IEEE Transactions on Antennas and Propagation

ideal case, still >13dB improvement is achieved over 4:1 bandwidth compared to the measured COTS circulators. If the hybrids, phase matched circulators, and interconnects are monolithically integrated, the isolation will be further enhanced. Since the same antenna is used as transceiver, the far-field performances of modes 1 TX and mode 1 RX are quite similar. To quantitatively characterize the similarity between the TX's and RX's radiation patterns over the operational bandwidth, a parameter called envelope correlation coefficient (ECC) is used [22]. Overall ECC >95% is obtained over the entire band. Therefore, only the TX side's performance is presented herein. The measured and simulated realized gain and axial ratio are shown in Fig. 8. As seen, the realized gain at broadside is >3.8dB over most of the band with excellent axial ratio <3dB up to elevation angles of 30° off broadside are obtained throughout 4:1 bandwidth. The measured and simulated co-polarized (RHCP) shows high quality mode 1 radiation patterns over the entire bandwidth (Fig. 9).

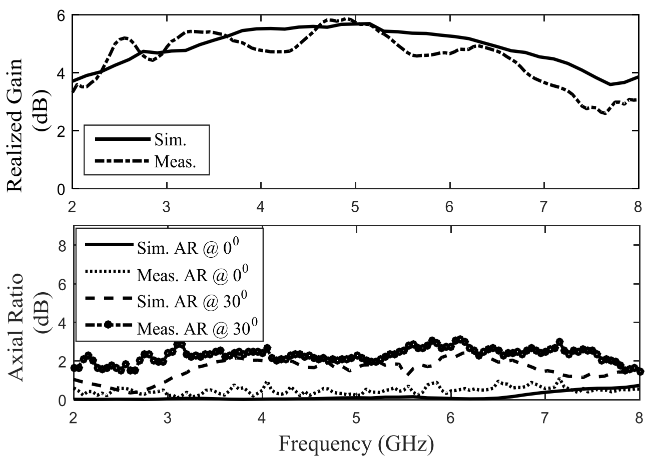

Fig. 8. Simulated and measured (a) realized gain of the four-arm spiral antenna in mode 1 and (b) axial ratio at $\theta = 0°$ and 30°.

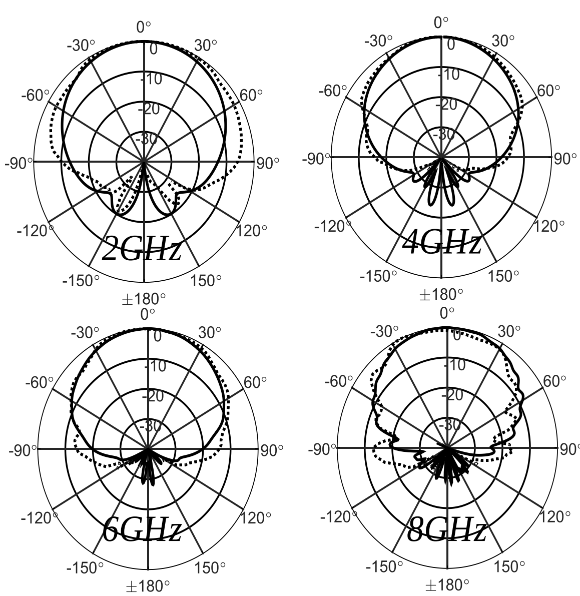

Fig. 9. Simulated (solid) and measured (dotted) normalized RHCP far-field radiation patterns of the TX/RX STAR four-arm spiral antenna.

V. Multimode STAR Antenna Subsystem Performance

The measured and simulated active matches of mode 2, mode 3, and mode -1 are shown in Fig. 10. As seen, the VSWR is <2 for mode 2 after ~3GHz-3.5GHz (almost 2 times the turn-on frequency of mode 1), whereas Mode 3 turns-on at ~4.5GHz, while mode -1 operates from ~2-4.3GHz (below the turn-on of mode 3). Further improvement in VSWR<1.7 for mode -1 and mode 3 is obtained once the antenna is connected to the complete circulator-BFN. The measured isolation for different cases is shown in Fig. 11. The measured isolation is >27dB (maximum of 38dB) over the band with a nominal of 32dB over the band for mode 1 TX/mode 2 RX. For mode 3 TX/mode 3 RX and mode -1 TX/mode -1 RX configurations, the isolation is >24dB (maximum of 35dB) with nominal of 30dB over the band. Improvement in isolation of >12dB and >15dB are achieved for mode 3 and mode (2,-1); respectively, compared to the stand-alone circulator's isolation.

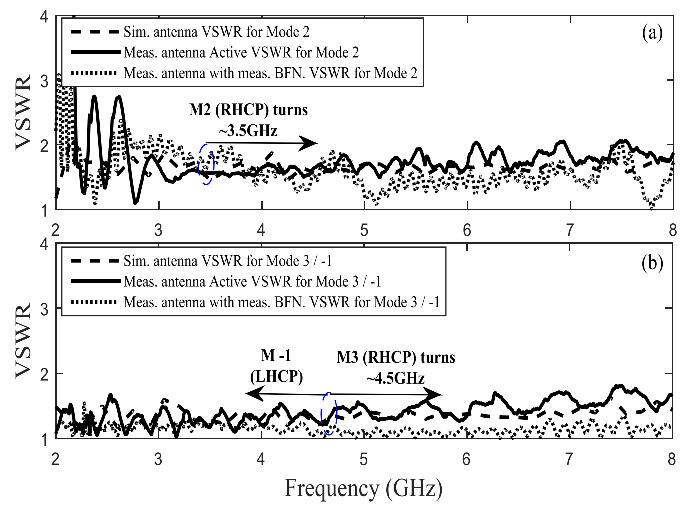

Fig. 10. Simulated and measured active VSWRs for the antenna and the TX/RX circulator-BFN's ports including the antenna: (a) Mode 2 and (b) mode 3 and mode -1.

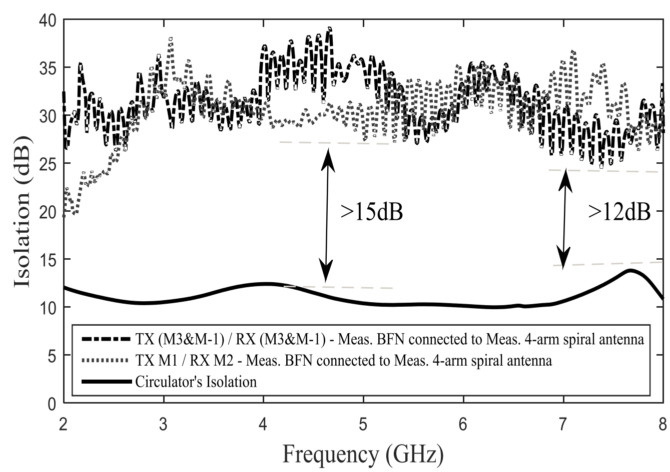

Fig. 11. Measured isolation between the TX/RX BFN's ports for RHCP Mode 3 TX / Mode 3 RX in ~4 GHz -8GHz, and LHCP Mode -1 TX / Mode -1 RX in 2GHz - ~3.9GHz range. Also shown is Mode 1 TX / Mode 2 RX measured isolation between the TX/RX BFN's ports (3.5GHz-8GHz).

The measured and simulated far-field performances are obtained for mode 2 (RHCP), mode -1 (LHCP), and mode 3

This article has been accepted for publication in a future issue of this journal, but has not been fully edited. Content may change prior to final publication. Citation information: DOI 10.1109/TAP.2017.2670362, IEEE Transactions on Antennas and Propagation

(RHCP). The axial ratio for mode 2 is measured at the peak gain elevation angle of 36°. As shown in Fig. 12, the achieved axial ratio is less than 4.2dB over (4.7-5.2GHz and 6-6.2GHz) and less than 3dB over most (84%) of the designated bandwidth of operation 3.5GHz-8GHz. Mode 3 on the other hand has an axial ratio at the peak gain of 48° less than 4dB over frequency band of 4.5GHz-8GHz; while mode -1 (LHCP) has an axial ratio less than 3dB over 2-4.2GHz at 0°. Overall, good circularly polarized performance is achieved with this fabricated four-arm multimode spiral. The realized gain over the specified operational band for mode 2, mode 3, and mode -1 is >2dBic, >1.2dbic, >1.5dBic, respectively.

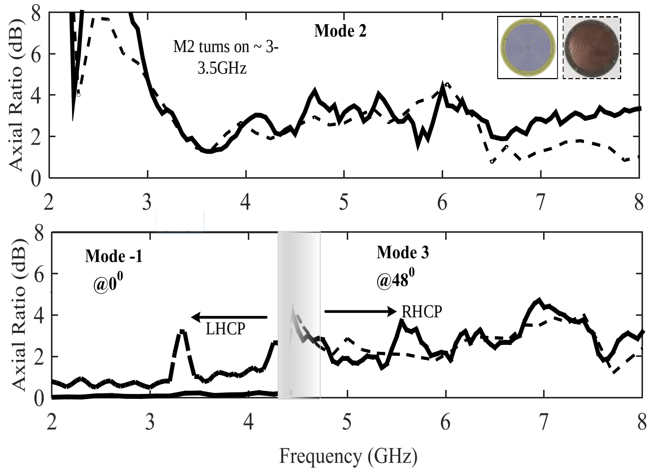

Fig. 12. Simulated and measured axial ratio of the four-arm spiral antenna at θ equals 36° for Mode 2 (RHCP), 0° for Mode -1 (LHCP), and 48° for Mode 3 (RHCP). (Simulated antenna is backed with ideal absorber).

Figs. 13, 14, and 15 show the plotted far-field patterns for the mode 2, mode -1, and mode 3 at different frequencies. The power loss of the complete beamformer is dependent on the match of the four-arm spiral and the leakage from the circulators.

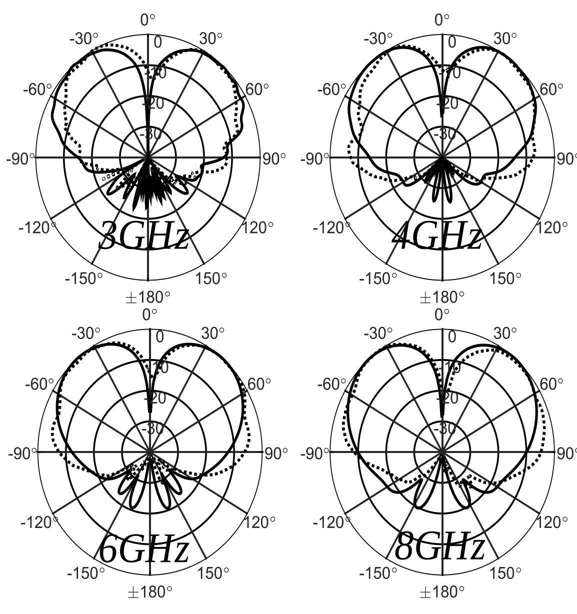

Fig. 13. Mode 2 simulated (solid) and measured (dotted) RHCP far-field radiation patterns of the STAR four arm spiral antenna.

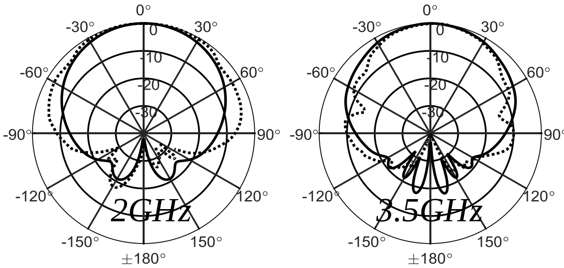

Fig. 14. Mode -1 simulated (solid) and measured (dotted) LHCP far-field radiation patterns of the STAR four arm spiral antenna. Only at lower frequency band (below 4GHz).

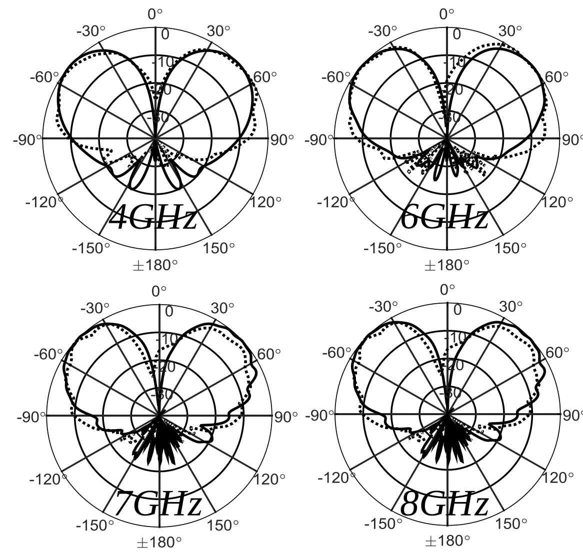

Fig. 15. Mode 3 simulated (solid) and measured (dotted) RHCP far-field radiation patterns of the STAR four arm spiral antenna. Only at higher frequency band (higher than 4GHz).

The measured power loss of the Butler-BFNs once connected to the measured antenna is shown in Fig. 16. The inherent loss of this feeding network is within 10%-20% for all different mode configurations. This loss can be further reduced and overall system performance improved with custom made, tight tolerance components/integrated networks. Finally, throughout this paper the computational predictions agree well with experiments indicating the robustness of the proposed concept.

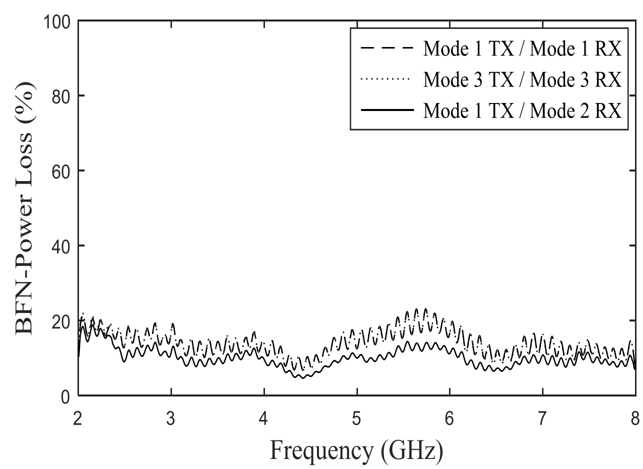

Fig. 16. The measured power loss of the STAR BFN once it is connected to the measured circulators and spiral antenna.

VI. Conclusion

A novel wideband multimode monostatic STAR antenna subsystem is introduced. The configuration is composed of a single four-arm spiral with four circulators, and two Butler matrix BFNs. It is theoretically demonstrated that infinite isolation between the TX and RX ports without any need for duplexing in time, frequency, polarization, or spatial domains is possible with ideal conditions. Moreover, the flexibility of achieving diverse circularly polarized mode combination (broadside and split-beam modes or RHCP and LHCP) using a single aperture while maintaining reasonable isolation over a wide bandwidth is demonstrated. High-simulated isolation is achieved for all mode arrangements (1, 2, 3, and -1). The proposed theoretical baseline used to explain the isolation phenomenology is fully confirmed with these results. The measurements on a concept demonstrator are carried out to experimentally prove the proposed concept. Results show isolation between 23 and 38dB for different mode arrangements. The obtained data emphasize the significance of imbalances and even though the theoretical isolation is compromised in the presence thereof more than 12dB improvement is still seen compared to the inherent COTS circulator isolation. All modes have shown to have good quality radiation patterns. Specifically, modes 1 and -1 have AR < 3dB over large field-of-view; while modes 2 and 3 measure AR levels at <4dB at the peak gain of 36° and < 4.2dB the peak gain of 48°, respectively.

References

[1] S. Chen, S. Sun, Y. Wang, “A Comprehensive Survey of TDD-Based Mobile Communication Systems from TD-SCDMA 3G to TDLTE(A) 4G and 5G directions,” *IEEE China Comm.,* Feb 2015, vol. 12, no.2, pp. 40-60.

[2] D. Esser, B. Solan and A. Chaloupka, “Improved antenna isolation in transmit/receive applications”, *Proc. GeMiC,* Karlsruhe, Germany, 2006.

[3] B. Chiang and M. Holdip, “Progressively Phased Circular Arrays Used in Antenna Isolation,” *IEEE Antennas and Propag. Soc. Int. Symp.,* Jun. 1974, vol.12, pp. 289-292.

[4] J. Choi, M. Jain, K. Srinivasan, P. Levis, and S. Katti, “Achieving Single Channel, Full Duplex Wireless Communication*,” The 16th Annual Int. Conf. on Mobile Comp. Net.*, Chicago, IL, July 2010, pp. 1-12.

[5] A. Sabharwal, P. Schniter, D. Guo, D. W. Bliss, S. Rangarajan, and R. Wichman, “In-Band Full-Duplex Wireless: Challenges and Opportunities*,” IEEE Trans. Selected Areas in Comm.,* Oct. 2014, vol. 32, no. 9, pp. 1637-1652.

[6] A. Khojastepour, K. Sundaresan, S. Rangarajan, X. Zhang, S. Barghi, "The Case for Antenna Cancellation for Scalable Full Duplex Communications." *ACM Workshop on Hot Topics in Networks,* Cambridge, MA, Nov. 2011.

[7] T. Snow, C. Fulton, and W. J. Chappell, “Multi-antenna Near Field Cancellation Duplexing for Concurrent Transmit and Receive*,” IEEE MTT-S Int. Microwave Symp.,* Baltimore, MD, June 2011, pp. 1-4.

[8] K. E. Kolodziej, P. T. Hurst, A. J. Fenn, and L.I. Parad, “Ring Array Antenna with Optimized Beam former for Simultaneous Transmit and Receive,” *IEEE Antennas Propag. Soc. Int. Symp.,* Chicago, IL, July 2012, pp. 1-2.

[9] A.T. Wegener and W. J. Chappell, “Simultaneous Transmit and Receive with a Small Planar Array,” *IEEE MTT-S Int. Microwave Symp.,* QC, Canada, June 2012, pp. 1-3.

[10] K. E. Kolodziej, B. T. Perry, “Simultaneous transmit and receive (STAR) mobile testbed,” *Radio and Wireless Symposium (RWS) IEEE*, Jan. 2016, pp. 66-69.

[11] S. Tang, C. Lin, and S. Hung, “Ultra-Wideband Quasi-Circulator Implemented by Cascading Distributed Balun With Phase Cancelation Technique,” *IEEE Trans. on Micr. Theory and Techniques,* July. 2016, vol. 64, no. 7, pp. 2014-2112.

[12] DITOM Microwave Inc., CA, USA. [Online]. Available: https://www.ditom.com/single_junction_circulators.php.

[13] J. L. Young, R. S. Adams, B. O'Neil, and C. M. Johnson, “Bandwidth Optimization of an Integrated Microstrip Circulator and Antenna assembly: Part 1,” *IEEE Antennas Propag. Mag*., 2007, vol. 49, no.1, pp. 82-91.

[14] R. S. Adams, B. O’Neil, and J. L. Young, “The Circulator and Antenna as a Single Integrated System,” *IEEE Antennas and Wireless Propag. Letters*, April 2009, vol. 8, pp. 165-168.

[15] W. Kim, M. Le, J. Kim, H. Lim, J. Yu, B. Jang, J. Park, “A Passive Circulator with High Isolation using a Directional Coupler for RFID,” *IEEE MTT-S Int. Microwave Symp.*, San Francisco, CA, June 2006, pp. 1177 – 1180.

[16] S. L. Karode and V. F. Fusco, “Feedforward Embedding Circulator Enhancement in Transmit/Receive Applications,” *IEEE Microwave and guided wave let.*, Jan 1998, vol. 8, no.1, pp. 33-34.

[17] S. K. Cheung, T. P. Halloran, W. H. Weedon, and C. P. Caldwell, “MMIC-Based Quadrature Hybrid Quasi-Circulators for Simultaneous Transmit and Receive,” *IEEE Trans. Microw. Theory Tech.,* March 2010, vol. 58, no. 3, pp. 489-497.

[18] M. J. Cryan, P. S. Hall, K. S. H. Tsang, and J. Sha, “Integrated active antennas with simultaneous transmit-receive operation,” *IEEE Microwave Conf., 26th European,* Prague, Czech Republic, Sep. 1996, vol. 2, pp. 565-568.

[19] C. Kalialakis, M J. Cryan, P. S. Hall, and P. Gardner, “Analysis and Design of Integrated Active Circulator Antennas,” *IEEE Trans. on Microwave Theory and Tech.,* Prague, Czech Republic, Aug. 2002, vol. 48, no. 6, pp. 1017-1023.

[20] C. H. Cox and E. I. Ackerman, “Photonics for Simultaneous Transmit and Receive,” *IEEE MTT-S Int. Microwave Symp.,* Baltimore, MD, June 2011, pp. 1-4.

[21] D. S. Filipović, M. A. Elmansouri, and E. A. Etellisi, “On Wideband Simultaneous Transmit and Receive (STAR) With a Single Aperture,” *IEEE Antennas Propag. Soc. Int. Symp.,* in proc., Fajardo, Puerto Rico, July 2016.

[22] E. A. Etellisi, M. A. Elmansouri, and D. S. Filipović, “Wideband Monostatic Simultaneous Transmit and Receive (STAR) Antenna,” *IEEE Trans. Antennas Propag*., July. 2015, vol. 65, no.1, pp. 6-15.

[23] G. Lathikre, N. Jolivet, S. Nobilet, R. Gillard, and J. E Hilard, “A Novel Balanced Circulator for FDD MC-CDMA Communications,” *IEEE Microwave Conf., 34th European*, Amsterdam, The Netherlands, Oct. 2004, pp. 605-608.

[24] M. E. Knox, “Single Antenna Full Duplex Communications using a Common Carrier,” *IEEE Wireless Micro. Tech. Conf.*, Cocoa Beach, FL, Apr. 2012, pp. 1-6.

[25] D. S. Filipović and T. P. Cencich Sr., “Frequency independent antennas,” in *Antenna Engineering Handbook*, 4th ed. New York, USA: McGraw Hill, 2007, ch. 13.

[26] EM Software & Systems-S.A. (Pty) Ltd, Stellenbosh, South Africa, "FEKO- a comprehensive electromagnetic simulation software tool," Suite 6.3, http://www.feko.info, 2013.

[27] M. Radway and D. S. Filipović, “Four-armed spiral-helix antenna,” *IEEE Antennas Wireless Propag. Lett.*, vol. 11, pp. 338-341, 2012.